Journal of Applied Electrochemistry (2006) 36:131–137
DOI 10.1007/s10800-005-9024-8

Electrodeposition of cobalt on gold during voltammetric cycling

I. FLIS-KABULSKA
Institute of Physical Chemistry of the Polish Academy of Sciences, 01-224, Warsaw, Poland
Tel.: +48-22-343-3406; Fax: +48-22-632-5276; E-mail: ifkab@ichf.edu.pl

Received 7 January 2005; accepted in revised form 3 July 2005

Key words: cobalt electrodeposition, cyclic voltammetry, gold, hydrogen, STM/AFM

Abstract

Co was electrodeposited on Au(111) from solutions of $CoSO_4$ in 0.5 mM H_2SO_4. STM showed that the electrodeposition started at an underpotential of 0.26 V. In cathodic sweeps voltammograms exhibited a low cathodic peak C1 at an overpotential of 0.1 V and a large cathodic peak C2 at an overpotential above 0.2 V. From the cathodic charge it was estimated that at peak C1, the deposit was about one monolayer thick. AFM indicated the presence of flat deposits at peak C1, and of numerous islands at peak C2, demonstrating massive nucleation and growth at the latter peak. It is suggested that peak C1 may be associated with a hindrance of nucleation processes due to adsorption of chemical species, probably of hydrogen H_{ad}. During a reverse anodic sweep from C2, anodic peaks A1 and A2 were observed. Peak A1 was evidently associated with anodic oxidation of electrodeposited cobalt, whereas peak A2 at nobler potentials, probably resulted from oxidation of hydrogen, incorporated into the Co electrodeposit.

1. Introduction

The Co/Au system has been widely studied mainly in connection with the perpendicular magnetisation anisotropy (PMA) observed for some *N*/*F*/*N* sandwich structures, where *N* is a non-ferromagnetic noble metal such as copper, gold or platinum, and *F* is a ferromagnetic metal layer of *e.g.* cobalt or nickel a few atomic layers thick [1]. In Co/Au multilayers, Co layers of thickness in the nanometer range (below 5–6 atomic planes) exhibit a magnetisation perpendicular to the layer plane. However, above a critical thickness a phase transition takes place resulting in the magnetisation reorientation to the in-plane direction. PMA allows increase in the information density of the magnetic layers, and therefore, it is of great interest for high-density data storage [1–3].

Sandwiches of Co/Au(111) exhibiting PMA have been prepared by ultra-high vacuum techniques (molecular beam epitaxy (MBE), thermal evaporation, sputter deposition) [1–5] and by electrochemical methods [5–13]. The latter methods are simpler and provide the possibility of easier control of the amount of deposited material. It has also been reported [12, 13] that electrodeposited structures Cu/Co/Au(111) exhibit PMA of higher strength than that for layers grown by MBE.

Electrodeposition of Co on Au(111) from $CoSO_4$ solutions resulted in structures which exhibited PMA for a Co thickness up to about 2 monolayers (ML) in solution containing Cl^- anions, and to about 4–5 ML in solution with SCN^- anions [12]. Initial stages of Co electrodeposition were studied *in situ* with scanning tunnelling microscopy (STM) on Au(111) in acidic solutions [10, 11], and on Au(111) and Au(100) electrodes in neutral sulphate solutions [14]. The electrochemistry of nucleation and growth of Co deposits from chloride solutions (pH 9.5) has been described [15, 16]. The initial growth of Co on Au depends on the crystallographic orientation of the substrate [14] and on the electrochemical conditions. In chloride solutions of pH 9.5 underpotential deposition (upd) of Co occurred [15]; in neutral sulphate solutions upd was not observed [14]. Uhlemann et al. have found that the magnetic field strongly affects the electrodeposition of Cu/Co–Cu multilayers [17] in a citrate electrolyte and that of Co on Au film in acidified sulphate solution [18].

The magnetic properties of electrodeposited Co films can be correlated with their structure and plating conditions, as considered by Armyanov [19]. Vicenzo and Cavallotti [20] describe the effects of electroplating parameters on the structure and growth modes of Co. The solution pH is one of the most important parameters in determining the structure of Co; at pH <2.5, both α-Co (hcp) and β-Co (fcc) are formed, in the pH range 2.5–3.0 transition from β to α-Co occurs. Depending on pH and hydrolysis equilibria, three basic growth modes were identified as perpendicular, lateral and cluster growths [20].

The initiation and propagation of Co electrodeposition on Au has been extensively studied [11–18]. Allongue et al. [11] studied the electrodeposition of Co from acidic solutions at overpotentials and found that at small overpotentials the nucleation is driven by place exchange as in the ultra-high vacuum (UHV), and subsequent growth leads to ML-thick Co nanostructures on hcp regions of a reconstructed Au(111) surface. At larger overpotentials, Co films grow epitaxially in a layer-by-layer mode, and at still larger overpotentials (at least 0.25 V negative to the Nernst potential) Co bulk deposition takes place.

Cyclic voltammograms exhibit cathodic and anodic peaks. In cathodic scans the voltammograms may have two [18] or three peaks [12, 15, 16] and, in the subsequent anodic scans, they can have two [12] or three peaks [15, 16]. These peaks suggest different growth modes and different structures of the Co films.

In the present work it was intended to correlate voltammogram peaks with electrode processes and to examine whether the observed cathodic peaks can be referred to the morphology of Co electrodeposits on Au(111) in acidic sulphate solutions. Electrodeposits were examined using *in situ* scanning tunnelling microscopy (STM) and *ex situ* atomic force microscopy (AFM).

2. Experimental

Polycrystalline gold was used as a substrate for electrodeposition of Co. Gold was vapour deposited on glass for STM studies, and on mica for AFM studies. Electrochemical measurements for the characterisation of electrodeposition were performed on gold sheets from bulk metal. Before experiments, Au was flame annealed in a reducing flame to obtain the reconstructed Au(111) surface [13, 21–23].

Electrochemical measurements were performed at ambient temperature in the following solutions: 0.5 mM H_2SO_4, 3 mM $CoSO_4 + 0.5$ mM H_2SO_4, and 14.9 mM $CoSO_4 + 0.5$ mM H_2SO_4 of pH 3.0. The solutions were prepared from analytical grade reagents and double distilled water. Conventional measurements were carried out in solutions de-aerated by purging with argon. The measurements were performed in a conical glass vessel in which samples were clamped via a rubber washer to a hole of 6.4 mm diameter at the bottom. The potentials were measured and reported against a mercury sulphate electrode (MSE): $Hg|Hg_2SO_4|0.1$ M Na_2SO_4, $E°$ (MSE) = +0.650 V (NHE). Voltammetric sweeps were measured from the potential of 0.1 V (MSE) (surface of Au without oxides) in cathodic direction at the potential scan rates of 4–100 mV s^{-1}.

Electrodeposition of Co for STM studies was conducted in a non-deaerated solution of 3 mM $CoSO_4 + 0.5$ mM H_2SO_4. The morphology of electrodeposited Co was investigated *in situ* with the Electro-Chemical STM from Molecular Imaging Corporation. STM tips were prepared from a 0.25-mm thick PtIr wire by etching in 30% $CuCl_2$ and were finally isolated with Apiezon Wax. A PtIr wire also served as a counter electrode and as a reference electrode in the electrochemical cell of the microscope. The potential of the PtIr reference electrode was determined against the MSE and reported as such.

Ex situ AFM studies were performed with a TopoMetrix Discoverer TMX 2000 system, version 3.05. The microscope was operated in contact (repulsive) mode using a Si_3N_4 cantilever with a tip of 0.6-μm diameter and a 25-μm scanner.

3. Results

3.1. *Electrochemical measurements*

Figure 1 shows voltammograms measured on gold in 0.5 mM H_2SO_4 without and with 14.9 mM $CoSO_4$. Arrows indicate the equilibrium potential for the H_2/H^+ electrode in 0.5 mM H_2SO_4 ($E°_{H/H^+} = -0.827$ V (MSE)), and for the Co/Co^{2+} couple with 14.9 mM $CoSO_4$ [24] ($E°_{Co/Co^{2+}} = -0.981$ V (MSE)).

For cathodic sweeps, the current density of hydrogen evolution reaction (HER) in the Co^{2+}-free solution began to rise at an overpotential of $\eta = 0.04$ V, whereas the current density of the Co deposition in the Co^{2+}-containing solution started at an underpotential of $\varepsilon = 0.16$ V. In the Co^{2+}-free solution, the current density of HER did not show a hysteresis for the positive and negative sweeps. In the Co^{2+}-containing solution, cathodic current density after a sweep reversal was lower than the current density in the Co^{2+}-free solution. This indicates that HER on electrodeposited Co was slower than on Au. Evidently, cobalt increased the overpotential of hydrogen evolution in comparison with gold. Similar results are known for iron and nickel [25] belonging also to the VIII group of the periodic table.

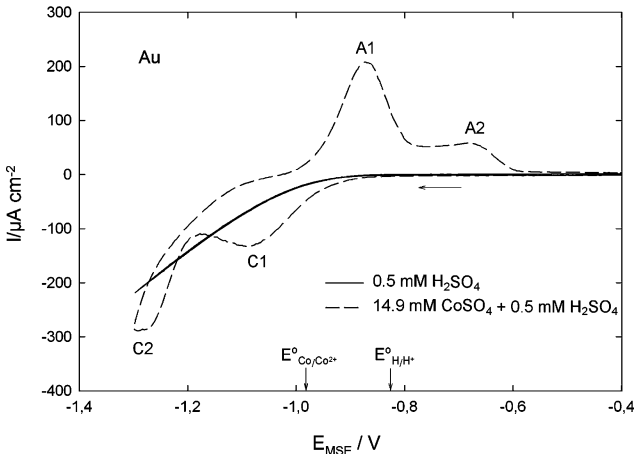

Fig. 1. Voltammograms on Au in 0.5 mM H_2SO_4 and in 14.9 mM $CoSO_4 + 0.5$ mM H_2SO_4, scan rate 25 mV s^{-1}. $E°_{H/H^+}$ and $E°_{Co/Co^{2+}}$ are equilibrium potentials in the solutions used.

The voltammogram in the Co^{2+}-containing solution exhibited two cathodic peaks (C1, C2) and two anodic peaks (A1 being larger than A2). In order to find a relationship between cathodic and anodic peaks, potential sweeps were reversed at different potentials. Figure 2 shows that anodic peaks started to appear only when the sweep was reversed in the region of peak C2, but not of peak C1. Peak A1 appeared earlier than peak A2; these peaks increased with the increasing cathodic potential of the reversal.

Peak A1 occurred at potentials above $E°_{Co/Co^{2+}}$, and is obviously associated with the anodic oxidation of the deposited cobalt:

$$Co = Co^{2+} + 2e^- \quad (1)$$

Peak A2 cannot be associated with an anodic oxidation of Co^{2+}, because the oxidation to Co^{3+} or Co^{4+} species in a solution of pH 3 is thermodynamically possible only at potentials above +0.6 V (MSE) [24]. It is suggested that A2 is associated with the oxidation of hydrogen which is absorbed and/or adsorbed on the electrodeposited Co. This process is possible, because A2 occurs above the equilibrium potential $E°^{+}_{H/H}$. Probably, only a part of the total amount of sorbed hydrogen is oxidised at peak A2; the rest can be released as H_2 during the anodic dissolution of Co at peak A1.

Figure 3 illustrates the effect of the potential scan rate on the voltammograms. The cathodic peak C1 and the anodic peak A1 increased with the increasing scan rate. Current density maxima I_{C1} at C1 are presented as a function of square root of the scan rates in Figure 4(a), and cathodic charges Q_{C1} (at peak C1) and Q_{SC2} (at the start of peak C2, i.e. at about −1.2 V) are presented in Figure 4(b). Q_{C1} and Q_{SC2} were obtained by integration of the cathodic currents; they include Co electrodeposition and HER.

Linear dependence of I_{C1} vs. $(dE/dt)^{0.5}$ for scan rates from to 49 mV s^{-1} suggests a diffusion control. The voltammograms indicate that the system is not reversible, nevertheless an approximate value of the diffusion coefficient was calculated from the equation for reversible systems at 25 °C [26]:

$$i_p = (2.69 \times 10^5) n^{3/2} A D_o^{1/2} C_o v^{1/2} \quad (2)$$

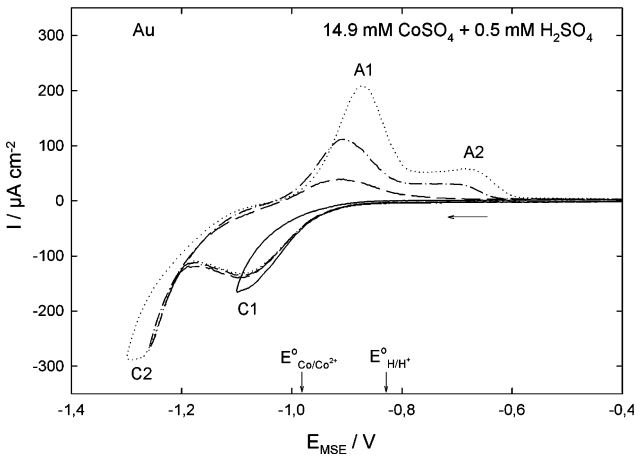

Fig. 2. Voltammograms on Au in 14.9 mM $CoSO_4$ + 0.5 mM H_2SO_4 for scan reversals at different potentials; scan rate 25 mV s^{-1}.

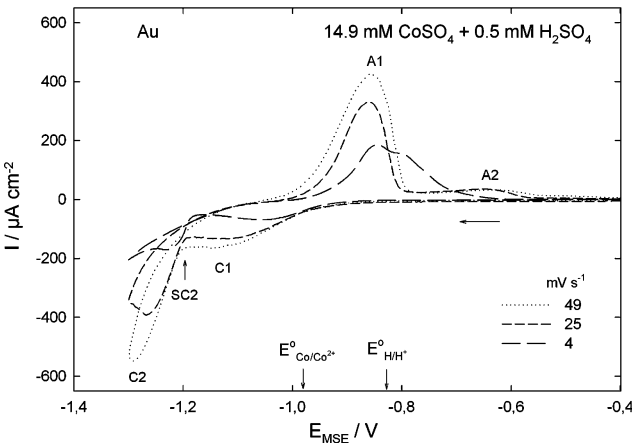

Fig. 3. Voltammograms on Au in 14.9 mM $CoSO_4$ + 0.5 mM H_2SO_4 measured at different potential scan rates (second scans are shown).

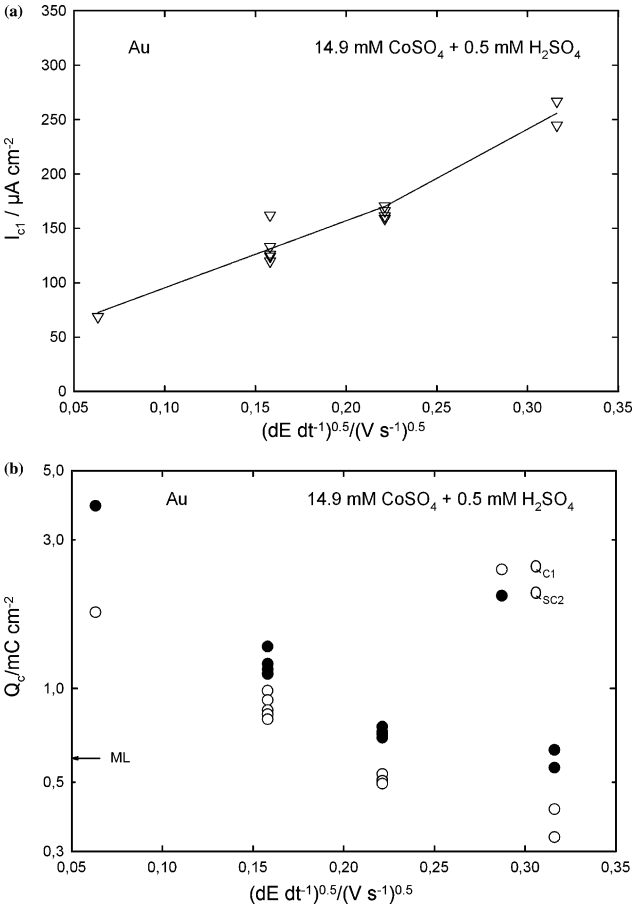

Fig. 4. Data from Figure 3: (a) current maxima I_{C1} at peak C1, (b) cathodic charge Q_{C1} at peak C1 and Q_{SC2} at the start of peak C2 (SC2) vs. square root of the scan rates. ML denotes the charge (0.59 mC cm^{-2}) for deposition of 1 ML of Co [13].

where i_p is the peak current in A, n is the stoichiometric number of electrons, A is the surface area in cm^2, D_o is the diffusion coefficient in $cm^2\ s^{-1}$, C_o is the concentration in mol cm^{-3}, and ν is the potential scan rate in $V\ s^{-1}$. From this equation one obtains $D_o \cong 3\times 10^{-9}\ cm^2\ s^{-1}$, which is by about 3 to 4 orders of magnitude lower than typical values for diffusion coefficients in aqueous solutions (5×10^{-6} to $10^{-5}\ cm^2\ s^{-1}$). This suggests that the diffusion control was associated with diffusion of electrodeposited species on the metal surface rather than with diffusion of Co^{2+} ions in the solution.

Cagnon et al. [13] indicate that the electric charge for deposition of a monolayer (ML) of Co with a surface atom density of $1.85\times 10^{15}\ cm^{-2}$ for Co(0001) corresponds to $0.59\ mC\ cm^{-2}$. This value is marked in Figure 4(b). A total charge involving deposition of 1 ML of Co and in addition HER (Figure 1) will be larger. Figure 4(b) shows that approximately such charges were observed for Q_{C1} measured at $49\ mV\ s^{-1}$, and for Q_{SC2} measured at $100\ mV\ s^{-1}$. On the basis of these charges it can be suggested that peak C1 is associated with the electrodeposition of approximately 1 ML of Co at the high scan rates.

The amount of electrodeposited metals can be evaluated by anodic stripping [10, 11]. However, this method appears to be less sensitive for detection of small amounts of electrodeposited Co than are cathodic currents. Figure 5 shows current densities for anodic sweeps from various potentials below $E°_{Co/Co^{2+}}$ at which electrodeposition of Co was conducted for 2 min. Loops of anodic currents above the potential of −0.9 V (MSE) are associated with the reaction of $Co \Rightarrow Co^{2+} + 2\ e^-$. These loops appeared after polarisation at −1.15 V (MSE) and below, but no sign of anodic oxidation was observed after polarisation at −1.10 V, corresponding to the overpotential for Co electrodeposition $\eta = 0.12$ V. Apparently the anodic stripping did not reveal Co deposition at overpotentials up to $\eta \approx 0.12$ V, whereas

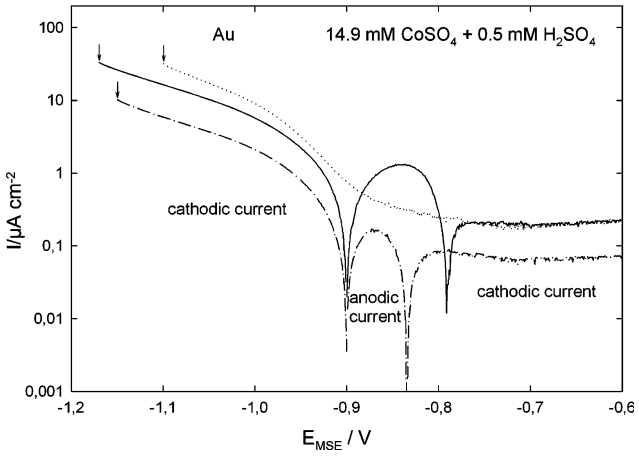

Fig. 5. Anodic scans after 2-min holding at potentials shown by arrows (−1.10, −1.15 and −1.17 V (MSE)); scan rate 1 mV s^{-1}. Anodic loops are associated with anodic oxidation of electrodeposited Co.

the cathodic sweeps revealed the start of electrodeposition at the underpotential $\varepsilon = 0.16$ V (Figure 1).

3.2. *STM examinations*

The surface of a gold film after flame annealing, with a preferential (111) orientation [13, 21–23], is shown in Figure 6(a). Typical for such a surface are flat terraces with steps of monoatomic height of about 0.2–0.3 nm.

Electrodeposition of cobalt was conducted in 3 mM $CoSO_4$ + 0.5 mM H_2SO_4 with $E°_{Co/Co^{2+}} = -1.001$ V (MSE) [24]. Figure 6(b) shows deposits of Co in form of small islands (dots), formed at $E = -0.74$ V within 17 min. This demonstrates that Co was deposited at the underpotential $\varepsilon = 0.26$ V. The islands were monoatomic in height and about 1–2 nm wide. On a few sites, some linear arrays of three or more islands can be seen.

At a potential of −0.84 V, small islands appeared after 1 min, and their number increased with time as shown in Figure 7. Initially, their number increased linearly with time, but after about 5 min. the formation of the islands was considerably accelerated. The size of these deposits appeared to remain unchanged, suggesting that they were the nucleation centres. At more negative potentials the nucleation centres were larger, e.g. after 1 min at $E = -0.94$ V (MSE) they were up to about 3 nm wide and about 1 nm high, but their number was similar to that at $E = -0.84$ V. This suggests growth of the cobalt islands.

3.3. *AFM examinations*

AFM was used to characterise the topography of Co deposits. A Au/mica substrate was polarised in 3 mM $CoSO_4$ + 0.5 mM H_2SO_4 by a cathodic sweep at a scan rate of $5\ mV\ s^{-1}$ from 0.2 V (MSE) to the potentials: $E°_{Co/Co^{2+}} = -1.00$ V, to peak C1 at $E = -1.18$ V and to the onset of peak C2 at $E = -1.23$ V. The voltammogram and the potentials chosen are shown in Figure 8. After attainment of these potentials, the samples were washed in water, dried and examined with AFM *ex situ*.

The AFM images are shown in Figure 9. Similarly as observed by STM (Figure 6(a)), the surface of annealed Au was characterised by flat terraces with about 0.5-nm high steps (Figure 9(a)). At $E = E°_{Co/Co^{2+}}$, bright spots appeared on the surface (Figure 9(b)), which are interpreted as islands of electrodeposited Co. They were about 0.5 nm high and 50 nm wide. Similar to the STM results of Figure 6(b), AFM suggests that at low potentials the electrodeposition of Co occurs in form of islands.

At peak C1, rounded overlapping planes of height 1–2 nm were formed (Figure 9(c)). The topography of these planes suggests that they expanded by lateral growth.

At the starting potential of peak C2, the surface was highly irregular (Figure 9(d)), with deposits in a variety of shapes and sizes, including many approximately 3–4 nm high islands. This topography suggests the

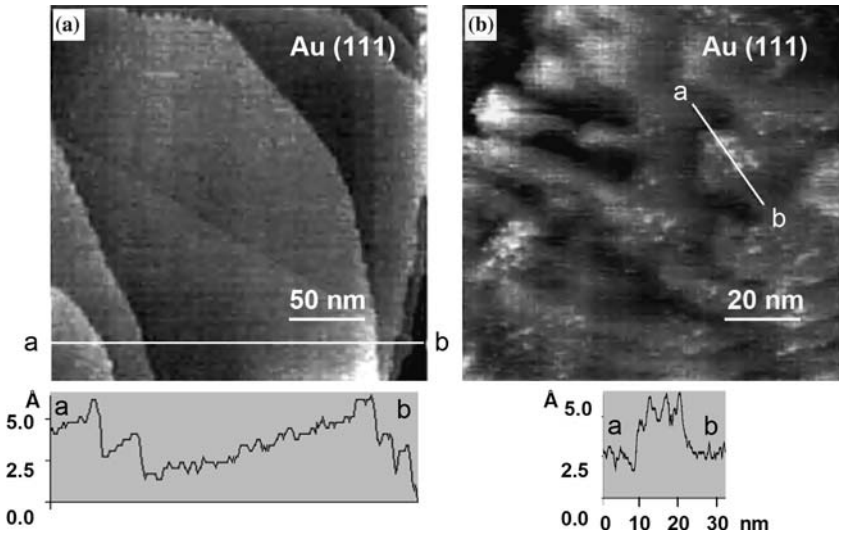

Fig. 6. STM images of the Au/glass substrate: (a) after annealing (terraces with steps about 0.2–0.3 nm high), (b) after a 17-min polarisation at −0.74 V (MSE) in 3 mM $CoSO_4$ + 0.5 mM H_2SO_4 (bright dots are Co islands).

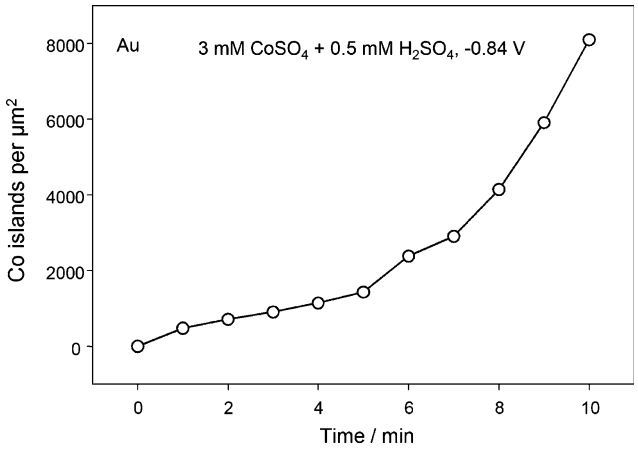

Fig. 7. Number of Co islands on gold as a function of the polarisation time in 3 mM $CoSO_4$ + 0.5 mM H_2SO_4 at −0.84 V (MSE).

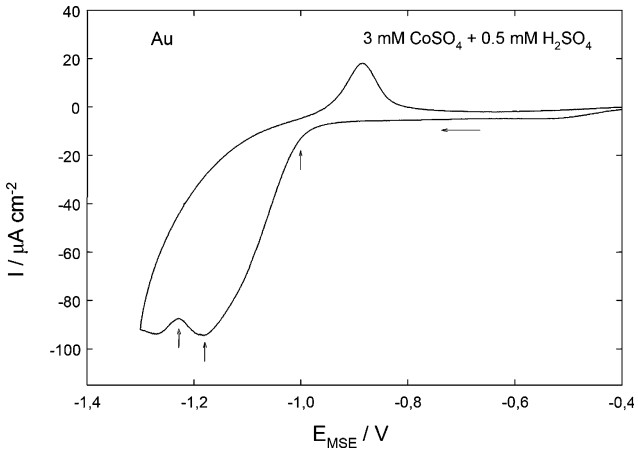

Fig. 8. Voltammogram on Au/mica in 3 mM $CoSO_4$ + 0.5 mM H_2SO_4, scan rate 5 mV s^{-1}; vertical arrows indicate the potentials (−1.00, −1.18 and −1.23 V (MSE)) of the AFM examination.

occurrence of a massive growth of Co deposits, involving random formation of islands.

4. Discussion

In the present work, upd of Co was observed by voltammetric cycling (Figure 1) and STM (Figure 6(b)). At the underpotential $\varepsilon = 0.26$ V, Co islands of atom-scale size (a few atoms wide, one atom high) were observed, some of them arranged in short straight lines. Linear arrays of deposited islands are characteristic for the UHV deposition; preferential formation of metal islands on Au (111) at the elbows of the herringbone reconstruction were observed for Co [27, 28], Fe [29] and Ni [30, 31]. Maybe, short linear arrays of electrodeposited Co islands show a tendency for a formation of the herringbone reconstruction.

Deposition at the Nernst potential (−1.00 V (MSE)) and at overpotentials (Figures 8 and 9) can be explained as described by Allongue et al. [11]. At the Nernst potential, small islands nucleate (Figure 9(b)), whereas at peak C1 rounded flat planes are formed (Figure 9(c)). They grow possibly by a layer-by-layer mode [11]. The average thickness of the layer at peak C1 can be estimated from the cathodic charge till the attainment of this peak; data in Figure 4(b) suggest that the layer is approximately one ML thick.

It is of interest, why the electrodeposition is slightly hindered after reaching peak C1 (Figures 1 and 8). It is supposed that one of the possible reasons is diffusion control of electrodeposited species (Co adatoms) on the metal surface during lateral growth. Diffusion control is suggested by a very low diffusion coefficient (about 3×10^{-9} cm^2 s^{-1}) evaluated from data in Figure 4(a). Another reason may be the hindrance of nucleation of islands. Possibly, a suggested hindrance of diffusion and/or nucleation may be associated with adsorption of

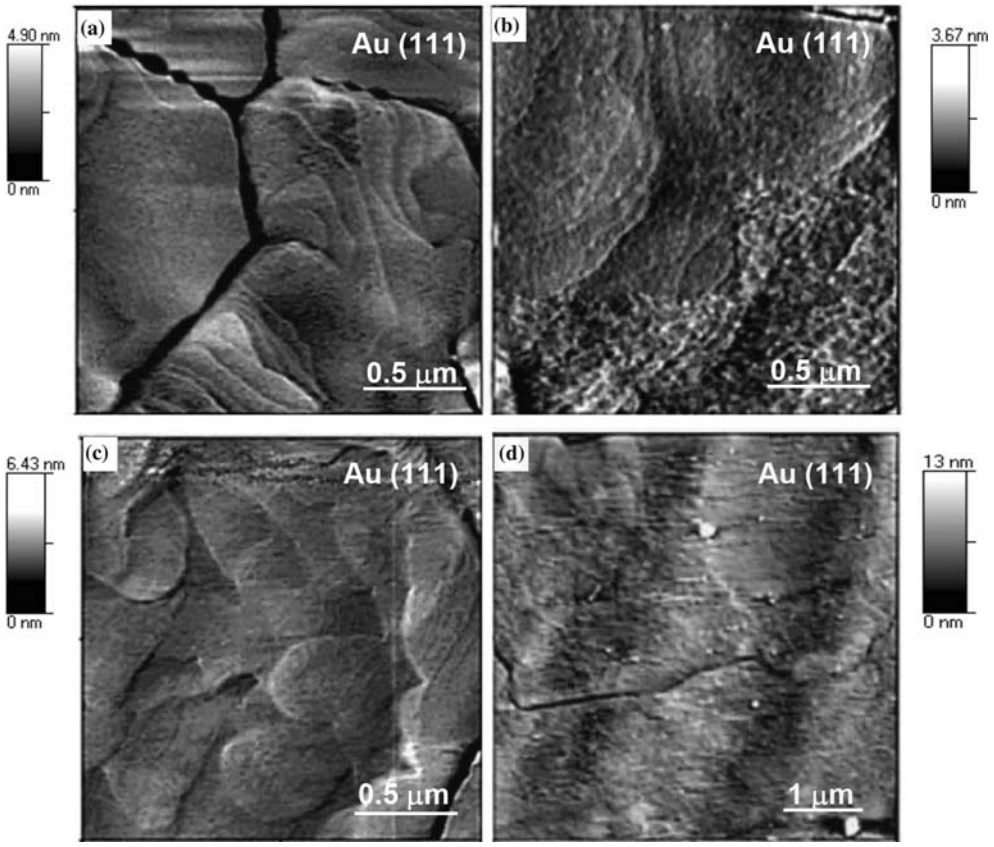

Fig. 9. AFM images of flame annealed Au/mica: (a) after annealing (terraces with steps about 0.5 nm high); (b–d) after a cathodic sweep in 3 mM $CoSO_4$ + 0.5 mM H_2SO_4 to potentials of (b) $E^{\circ}_{Co/Co^{2+}}$ (−1.00 V (MSE)), islands of Co were formed; (c) of peak C1 (−1.18 V), rounded flat planes were formed, with steps about 1–2 nm high; (d) beginning of peak C2 (−1.23 V), numerous small and large islands suggest a massive nucleation and growth.

chemical species on the deposited metal. Vicenzo and Cavallotti [20] explained various growth modes of Co by adsorption of hydrolysed species, or of complexes stabilised by boric acid. In the solution used in the present work (sulphate anions, pH 3), hydrogen H_{ad} may be involved as an adsorbed species, because HER occurs simultaneously with Co electrodeposition (Figure 1).

The abrupt rise in cathodic current density at the beginning of peak C2 (Figures 1–3) starts at the overpotential $\eta \approx 0.2$ V almost independently of the scan rate (Figure 3). Many Co islands and large deposits (Figure 9(d)) suggest that rapid nucleation took place at this potential, followed by bulk growth. The growth mechanism at large overpotentials has been extensively studied and discussed [11].

It is characteristic that the increase of peak C2 is accompanied by the increase of anodic peak A2 (Figure 2). For thermodynamic reasons [24], the latter peak cannot be ascribed to oxidation of Co^{2+}. Therefore, it is suggested that peak A2 is associated with anodic oxidation of incorporated hydrogen.

The possible incorporation of hydrogen into the electrodeposited Co can be suggested on the basis of studies by other authors. Nishiue et al. [32] studied thermal desorption of hydrogen from the cathodically charged intermetallic compound Co_3 Ti and suggested that hydrogen was trapped in interstitial sites of the $L1_2$ lattice and at grain boundaries. Co does not form hydrides under normal conditions, but the formation of hydrides is possible under high pressures; Antonov et al. [33] obtained an H/Co atomic ratio of about 0.95 in $Co_{99.8}Fe_{0.2}$ alloy at 325 °C under pressures of 4–6 GPa. Formation of molecules of Co hydrides CoH, CoH_2 and CoH_3 was observed in a high electric field of 15–20 V nm^{-1} [34]. Figure 1 shows that the HER current was sufficiently high to assure entry of hydrogen into the electrodeposit.

5. Conclusions

This study of Co electrodeposition on Au(111) from $CoSO_4$ solutions in 0.5 mM H_2SO_4 showed the following:

STM examination revealed that electrodeposition of Co on Au occurred at a potential which is by 0.26 V more positive than the Nernst potential; this denotes the underpotential deposition (upd). Upd deposits had the shape of islands of an atom- or nano-scale size.

During cathodic sweeps, peak C1 occurred at an overpotential of about 0.1 V, and peak C2 started to grow at an overpotential of about 0.2 V. At peak C1,

rounded flat planes of the Co deposit were formed. From the voltammograms it was deduced that the average thickness of the deposit was approximately one monolayer. At peak C2, massive electrodeposition occurred. Many Co islands and large deposits suggest that rapid nucleation takes place, followed by bulk growth. It is suggested that peak C1 may be associated with the hindrance of the surface diffusion of Co adatoms and of nucleation processes, due to the adsorption of chemical species, mainly of hydrogen H_{ad}. Based on the growth mechanisms studied in [11], peak C1 may be attributed to the layer-by-layer growth mode, as observed in [11] at low overpotentials.

During the reverse anodic sweep, peak A1 is associated with anodic oxidation of electrodeposited cobalt, whereas peak A2 at nobler potentials is probably associated with anodic oxidation of hydrogen, incorporated into the Co electrodeposits at peak C2.

Acknowledgment

The author thanks Dr. M. Uhlemann in the Institute of Solid State and Materials Research, Dresden, Germany, for her contribution to the STM study and for critical remarks.

References

1. W.J.M. de Jonge, P.H.J. Bloemen and F.J.A. den Broeder, *in* J.A.C. Bland and B. Heinrich (Eds), 'Ultrathin Magnetic Structures' Vol. 1 (Springer-Verlag, Berlin/Heidelberg, 1994) p. 65.
2. M. Mansuripur, *The Physical Principles of Magneto-Optical Recording* (Cambridge University Press, London, 1995).
3. F.J. Himpsel, J.E. Ortega, G.J. Mankey and R.F. Willis, *Vacuum* **46** (1995) 1133.
4. C. Chappert and P. Bruno, *J. Appl. Phys.* **64** (1988) 5736.
5. R. Allenspach, M. Stampanoni and A. Bischof, *Phys. Rev. Lett.* **65** (1991) 3344.
6. J.L. Bubendorff, E. Beaurepaire, C. Mény, P. Panissod J.P. Bucher, *Phys. Rev. B* **56** (1997) R7120.
7. J.L. Bubendorff, E. Beaurepaire, C. Mény, J.P. Bucher and P. Panissod, *J. Appl. Phys.* **83** (1998) 7043.
8. A. Gündel, A. Morrone, J.E. Schmidt, L. Cagnon and P. Allongue, *J. Magn. Magn. Mater.* **226–230** (2001) 1616.
9. S. Padovani, P. Molinas-Mata, F. Scheurer and J.P. Bucher, *Appl. Phys. A* **66** (1998) S1199.
10. A. Gündel, L. Cagnon, C. Gomes, A. Morrone, J. Schmidt P. Allongue, *Phys. Chem. Chem. Phys.* **3** (2001) 3330.
11. P. Allongue, L. Cagnon, C. Gomes, A. Gündel and V. Costa, *Surf. Sci.* **557** (2004) 41.
12. L. Cagnon, A. Gündel, T. Devolder, A. Morrone, C. Chappert, J.E. Schmidt and P. Allongue, *Appl. Surf. Sci.* **164** (2000) 22.
13. L. Cagnon, T. Devolder, R. Cortes, A. Morrone, J.E. Schmidt, C. Chappert and P. Allongue, *Phys. Rev. B* **63** (2001) article 104419.
14. M. Kleinert, H.-F. Waibel, G.E. Engelmann, H. Martin D.M. Kolb, *Electrochim. Acta* **46** (2001) 3129.
15. L.H. Mendoza-Huizar, J. Robles and M. Palomar-Pardavé, *J. Electroanal. Chem.* **521** (2002) 95.
16. L.H. Mendoza-Huizar, J. Robles and M. Palomar-Pardavé, *J. Electroanal. Chem.* **545** (2003) 39.
17. M. Uhlemann, A. Gebert, M. Herrich, A. Krause, A. Cziraki and L. Schulz, *Electrochim. Acta* **48** (2003) 3005.
18. A. Krause, M. Uhlemann, A. Gebert and L. Schulz, *Electrochim. Acta* **49** (2004) 4127.
19. S. Armyanov, *Electrochim. Acta* **45** (2000) 3323.
20. A. Vicenzo and P.L. Cavallotti, *Electrochim. Acta* **49** (2004) 4079.
21. R.J. Nichols, E. Bunge, H. Meyer and H. Baumgärtel, *Surf. Sci.* **335** (1995) 110.
22. J. Clavilier, R. Faure, G. Guinet and R. Durand, *J. Electroanal. Chem.* **107** (1980) 1205.
23. W. Haiss, D. Lackey, J.K. Sass and K.H. Besocke, *J. Chem. Phys.* **95** (1991) 2193.
24. M. Pourbaix, *Atlas of Electrochemical Equilibria in Aqueous Solutions* (Pergamon Press, Brussels, 1966), pp. 322.
25. P. Rüetschi and P. Delahay, *J. Chem.Phys.* **23** (1955) 195.
26. A.J. Bard and L.R. Faulkner, *Electrochemical Methods. Fundamentals and Applications* (J. Wiley & Sons, New York, 2001), pp. 231.
27. B. Voigtländer, G. Meyer and N.M Amer, *Phys. Rev. B* **44** (1991) 10354.
28. J. Wollschläger and N.M. Amer, *Surf. Sci.* **277** (1992) 1.
29. J.A. Stroscio, D.T. Pierce, R.A. Dragoset and P.N. First, *J. Vac. Sci. Technol. A* **10** (1992) 1981.
30. D.D. Chamliss, R.J. Wilson and S. Chiang, *Phys. Rev. Lett.* **66** (1991) 1721.
31. J.A. Meyer, I.D. Baikie, E. Kopatzki and R.J. Behm, *Surf. Sci.* **365** (1996) L647.
32. T. Nishiue, Y. Kaneno, H. Inoue and T. Takasugi, *Intermetallics* **11** (2003) 817.
33. F.E. Wagner, G. Grosse, M. Baier, V.E. Antonov and T.E. Antonova, . *J. Alloys Comp.* **239** (1996) 198.
34. B. Bialek and Z.M. Stepień, . *Vacuum* **63** (2001) 241.